An Evaluation of the Community Aerosol Inlet for the NCAR C-130 Research Aircraft

B. W. BLOMQUIST, B. J. HUEBERT, S. G. HOWELL, AND M. R. LITCHY*

Department of Oceanography, University of Hawaii, Honolulu, Hawaii

C. H. TWOHY,+ A. SCHANOT, AND D. BAUMGARDNER

Research Aviation Facility, National Center for Atmospheric Research, Boulder, Colorado

B. LAFLEUR AND R. SEEBAUGH

Department of Engineering, Denver University, Denver, Colorado

M. L. LAUCKS

Department of Chemical Engineering, University of Washington, Seattle, Washington

(Manuscript received 23 March 2000, in final form 11 September 2000)

ABSTRACT

Based on both in-flight measurements and a fluid dynamics model, airflow in the National Center for Atmospheric Research (NCAR) Community Aerosol Inlet (CAI) is similar to fully developed pipe flow. Distortions of the velocity field were pronounced when suction to inlet tubes was shut off, but conditions were otherwise insensitive to all flight parameters but airspeed. The principal value of the multiuser CAI system for NCAR's C-130 is that it decelerates air with no curves until the velocity has been reduced to 10 m s^{-1}. It then supplies uniformly modified air (after turbulent losses) to all users, enabling valid closure experiments.

Chemical data from both the First Aerosol Characterization Experiment (ACE-1) and the Second Community Aerosol Inlet Evaluation Program (CAINE-II) clearly indicate that while passing efficiency for submicron aerosol is acceptable, very little of the sea salt mode mass is transmitted by the CAI to instruments inside the aircraft. Comparisons between chemical samples from an external total aerosol sampler and samplers behind the CAI indicate that 70%–90% of the sea salt mass is unable to pass the CAI. The 50% cut size is about 3 μm, but the precise details of the efficiency curve are obscured by the difficulty of measuring a reference ambient aerosol distribution. The loss of particle mass becomes very significant above 3 μm, but the size cut is not sharp. These conclusions are supported by calculated particle transmission efficiencies for the CAI.

1. Introduction

The direct and indirect effects of atmospheric aerosols on radiative forcing are topics of intense interest and of direct relevance to climate change. They remain the greatest source of uncertainty in global climate models (IPCC 1995). Diverse origins and short lifetimes for atmospheric aerosols ensure that concentrations vary widely and fluctuate rapidly. As a result, measurements of aerosol characteristics from a wide variety of locations, during representative periods of the seasonal cycle, and throughout the air column, are necessary to determine both the nature of aerosols and the processes that control their production, transport, and deposition.

Obtaining a representative sample of the ambient aerosol size distribution is frequently difficult. Larger particles (>1 μm) are subject to variable and often poorly characterized losses on the inlet surfaces. These problems are exacerbated on aircraft by high airspeed (Baumgardner and Huebert 1993; Huebert et al. 1990; Sheridan and Norton 1998). A great variety of measurement systems, ranging from bulk filters to particle sizing instruments, are used on aircraft to examine ambient aerosols. Each of these has unique inlet requirements. Understanding the passing efficiency of the inlet is critical to a meaningful interpretation of aerosol data.

Known factors that contribute to inlet losses include variations in flow rate; orientation of the inlet relative to airflow streamlines; electrostatic effects; shadow

* CT Associates Inc., Bloomington, Minnesota.

+ College of Oceanic and Atmospheric Sciences, Oregon State University, Corvallis, Oregon.

Corresponding author address: Byron Blomquist, Department of Oceanography, University of Hawaii, 1000 Pope Rd., Honolulu HI 96288.
E-mail: byronb@soest.hawaii.edu

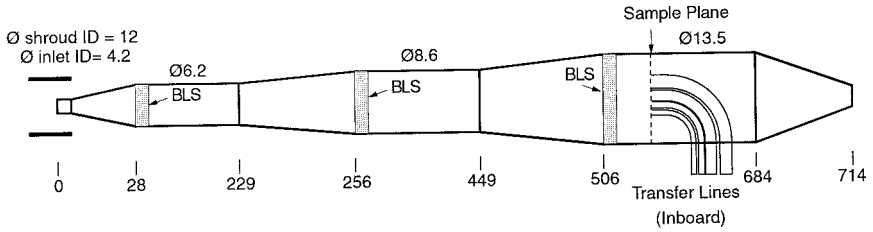

FIG. 1. Longitudinal diagram of the CAI (not to scale) showing the three diffuser cones and boundary layer suction vents (BLS), inlet shroud, and sample pickoff plane. Lengths and inner diameters are in centimeters. The bottom of the diagram is the inboard (aircraft) side.

zones created by the aircraft itself; flow separation and turbulence at the inlet and in transfer tubing; and deposition in bends in the transfer tubing. It is generally accepted that near-unit passing efficiency requires isokinetic, laminar flow, isoaxial to the external streamlines around the aircraft, surfaces free of electrostatic potential gradients, and bends with radii large enough to minimize losses at the design flow rate.

The Community Aerosol Inlet (CAI) on the National Center for Atmospheric Research (NCAR) C-130 research aircraft was built in the mid-1990s in response to the need of the aerosol research community to obtain representative aerosol samples during large, multiuser aircraft research programs. Design criteria were expected to optimize particle passing efficiency over a wide size range and included the following goals: (a) collect air from ahead of the aircraft fuselage, where flow distortion and shadowing effects are minimal; (b) decelerate air from approximately 120 m s^{-1} to 10 m s^{-1} gradually, rather than rapidly, to prevent flow separation; and (c) provide a capacity for sampling by up to 7 individual users with different flow rate requirements, with a total sampling capacity of 1000 L min^{-1}. The resulting inlet design is represented in (Fig. 1).

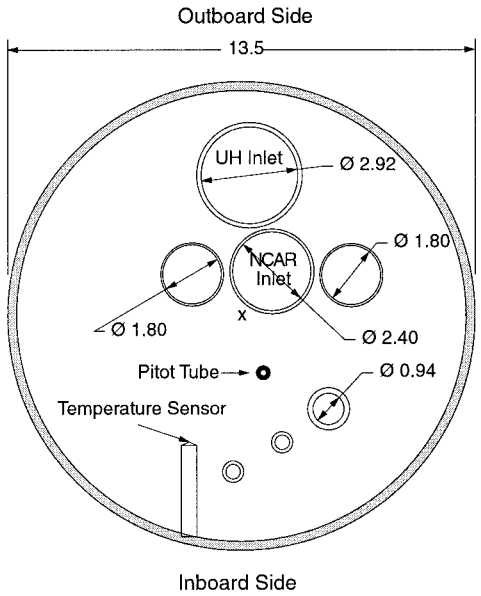

FIG. 2. Cross-sectional scale drawing of the CAI sampling plane showing the pickoff tubes, pitotstatic probe, and temperature sensor. Dimensions are in cm.

The CAI is a shrouded inlet with a total design flow rate of 8000 L min^{-1}. As such it samples a large quantity of undisturbed air, free of contamination from aircraft surfaces. The intent was to place the inlet tip in a region where the airflow would be aligned with the axis of the inlet, using a shroud to correct for minor nonisoaxiality. The shroud, however, does not incorporate sufficient leading edge bluntness to accommodate large incidence angles. Subsequent measurements have suggested that the tip flow may be nonisoaxial. Airflow decelerates through a series of three diffuser cones (cone angle = 5°) from 100 m s^{-1} to about 10 m s^{-1}. Straight sections were included between each diffusing stage to help prevent boundary layer separation. Seven curved pick-off tubes, located in a common plane across the flow, subsample the air and deliver it to instruments inside the aircraft (Fig. 2). Inside diameters of these tubes range from 0.44 to 2.92 cm, yielding isokinetic flow rates of 9 to 400 L min^{-1}. Boundary layer suction at the end of each diffuser cone, intended to minimize turbulence, removes a small portion of the flow upstream of the pick-off tubes. Subsequent testing of low turbulence inlets in the laboratory by coauthors Lafleur and Seebaugh has shown, however, that the suction scheme of the CAI is not sufficient to reduce turbulence significantly (as results from these tests will also show), and should have been applied within the diffuser rather than at the end.

The CAI was used to supply sample air to a variety of collection and sizing devices during two recent field programs focusing on aerosols: the First Aerosol Characterization Experiment (ACE-1) and the Indian Ocean Experiment (INDOEX). It is therefore important to evaluate the amount of bias the CAI imposes on ambient aerosol distributions.

The principal difficulty with in-flight evaluations of inlet performance is determining the reference (undisturbed ambient) aerosol distribution for comparison with that measured downstream of the inlet. Any device that relies on an inlet is potentially biased, including many optical particle counters. Inlet-less optical particle counters (OPCs) such as the forward scattering spectrometer probe (FSSP) do examine a nearly undistorted

distribution, but they suffer from the effects of Mie oscillations that become severe in the vicinity of one to several microns diameter. Samplers in which all inlet surfaces are extracted and analyzed can provide a defendable bulk concentration (and are used here), but they do not directly determine the size distribution of ambient particles. In some cases one can make comparisons with samplers on towers or ships, for which lower wind speeds make inlet losses less severe. However, questions inevitably arise about whether the aircraft and the surface sampler both measured exactly the same air. Several approaches are employed here to assess the ambient distribution. While none produced an unassailable reference aerosol spectrum, all suggest similar conclusions about the CAI passing efficiency.

Three flight programs have been conducted to assess the performance of the CAI. The first Community Aerosol Inlet Evaluation Program (CAINE) occurred in Colorado in 1995. At that time, in-flight comparisons between optical particle counters installed on a meteorological tower and behind the CAI inlet on the C-130 were used to estimate the passing efficiency for small particles. Late in 1995 we gathered more data during the ACE-1 experiment near Tasmania (Huebert et al. 1998). In May and June of 1997 additional test flights (CAINE-II) were conducted in Colorado and New Orleans.

During CAINE-II Colorado flights, air velocity and turbulence were measured across the sampling plane (where the pick-off tubes pull decelerated air into the fuselage) using a hot film anemometer. The effects of airspeed, pitch, yaw, pickoff tube flow, and boundary layer suction on the turbulence and velocity distribution were examined. To enable less costly evaluations of future modifications, the resulting data was used to test a fluid dynamics model of airflow in the CAI.

During subsequent CAINE-II flights from New Orleans, measurements of ambient seasalt aerosol were used to examine the passing efficiency of the CAI for supermicron particles. Chemical concentrations on a filter behind the CAI, on a 1-μm impactor behind the CAI, and on a reference external bulk sampler were compared. An Aerodynamic Particle Sizer (APS) (model 3320, Thermo Systems Inc.) was used to measure the aerosol size distribution behind the CAI while an external forward scattering spectrometer probe (FSSP-300, Particle Measuring Systems, Inc.) measured the ambient particle size distribution.

This paper presents results from the CAINE and ACE-1 field programs that characterize CAI performance and provide a basis for the further development of airborne aerosol inlets.

2. Velocity/turbulence measurements

Velocity and turbulence measurements were performed using hot film anemometry (Model 1053B anemometer and model 1260BS-10 platinum hot film probe, TSI, Inc.). An in-flight positioning device fabricated at Denver University allowed us to place the probe at various distances along several chords, 13 mm forward of the sampling plane. The sensor has a diameter of 60 μm and the sampling frequency was 5000 Hz. Calibration of the probe included a correction for temperature differences between the flow used for calibration and the measured flow. Turbulence intensity, I, is defined as the ratio of the square root of the mean-squared fluctuating velocity and the time averaged velocity,

$$I = \frac{\sqrt{(u')^2}}{\overline{u}}, \tag{1}$$

where u' are instantaneous deviations from the time averaged velocity.

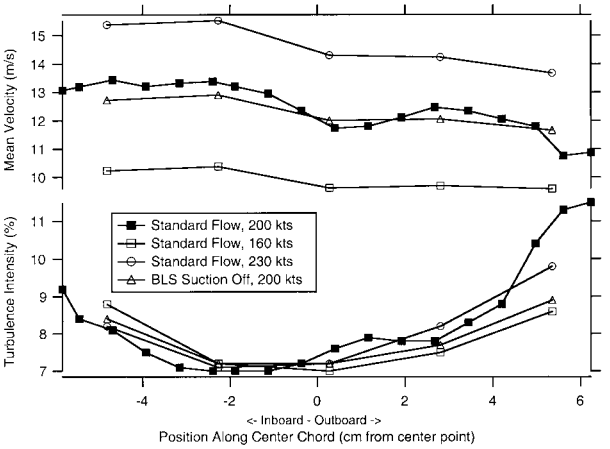

FIG. 3. Mean air velocity and turbulence intensity measurements made by hot film anemometry along the center chord of the sample pickoff plane (CAINE-II, Flight 3). Measurements were made at 160, 200, and 230 kt (indicated air speed: 200 kt = 102 m s^{-1}). Additional measurements were made at 200 kt with boundary layer suction in the diffuser cones shut off. Both velocity and turbulence were fairly uniform across the sampling plane. Boundary layer suction had a negligible effect.

Figure 3 shows that mean air velocity across the center chord of the sampling plane and away from the boundary layer varied smoothly as a function of airspeed and that turbulence intensity was also fairly constant across the center chord. The velocity distribution across the entire sampling plane was quite uniform (Fig. 4a). Flow at the sampling plane resembled fully turbulent pipe flow. Except for changes in flow velocity related to changes in airspeed, the velocity and turbulence intensity did not change significantly during pitch and sideship maneuvers. Airflow through the CAI exhibited a well-correlated deceleration from the free stream to the sample plane with a deceleration ratio of about 10:1. It is also apparent from Fig. 3 that modest flow (30 L min^{-1} or 0.4% of total flow) removed by boundary layer suction applied at the end of each diffuser cone had no detectable effect on flow velocity or turbulence in the CAI.

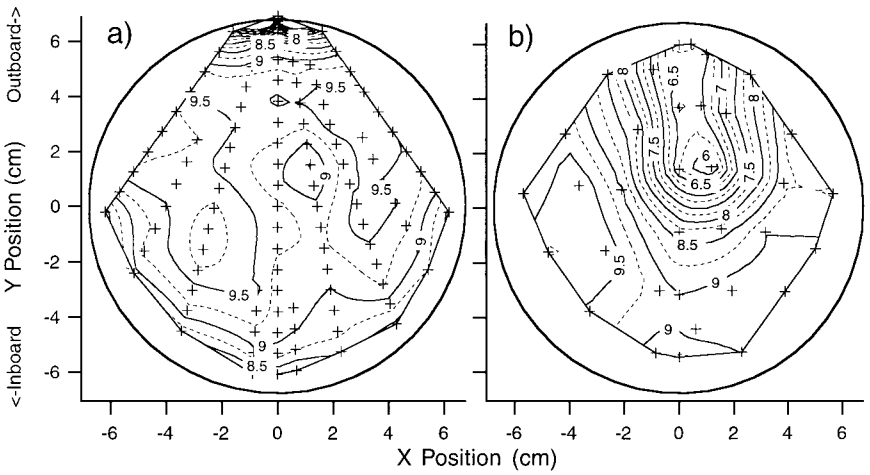

FIG. 4. Cross-sectional contour plots of measured mean velocity in the sample pick-off plane. Contour interval: 0.25 m s^{-1}. Crosses indicate measurement points. (a) Normal isokinetic flow in all pickoff tubes, 5000-ft altitude, 200 kt. (b) Same as in (a) but UH and NCAR pickoff flows off. The velocity probe was inserted from the outboard side. Compare with Fig. 2 for the position of inlets in the sampling plane.

Interrupting flow in pick-off tubes causes a significant perturbation to the overall flow (Fig. 4b). These results justify a policy requiring all users to maintain design flows, whether sampling or not. It is clear that shutting off or significantly changing any inlet flow causes neighboring tubes to become non-isokinetic.

3. Modeled flow and transmission efficiencies

Flow in one portion of the CAI was modeled using the Star-CD fluid dynamics computational package (Computational Dynamics Limited, distributed in the United States by Adapco, Melville, NY) at flow rates typical of in-flight use. Due to computational limitations for such a large structure, only the CAI sampling plane region was modeled (199 000 cells over a region upstream and downstream of the sample plane). The intent was to examine the extent of flow perturbation upstream of the sample plane caused by the presence of the pickoff tube bundle entering from the inboard side of the CAI. Measured velocities across the sample plane are used as a test of model accuracy. Assuming reasonable agreement with the measurements, the model is a valuable tool for studying the effects of modifications to the pick-off tube arrangement and may also provide a way to study particle trajectories near the sample plane. The upstream model boundary velocity was prescribed at 8.8 m s^{-1}, the mean measured velocity upstream of the sample plane. The model includes compressibility and viscous effects but heat exchange was not included. Figure 5 shows that flow velocity modeled with Star-CD agrees well with measured values across the center chord of the sample plane. Results for the upstream region confirm that flow distortion caused by the pickoff tube bundle is not a serious problem.

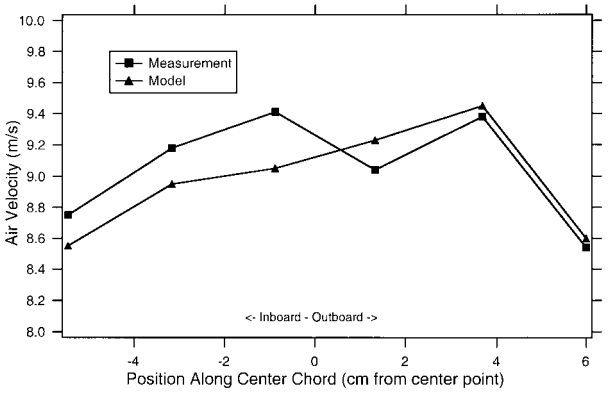

FIG. 5. Measured and modeled air velocity across center chord of the sampling plane in the CAI.

Aerosol loss processes in the CAI were also examined theoretically, though no existing theories are entirely valid for diffuser cones. Large particle losses may occur in the CAI due to non-isoaxial sampling at the inlet tip (Okazaki et al. 1987), turbulent deposition at high Reynolds number (Re), sedimentation, and deposition in bent tubes downstream of the sampling plane (Cheng and Wang 1977; Pui et al. 1987). The CAI's shroud (Torgeson and Stern 1966; Twohy 1998) was intended to straighten airflow and particle trajectories upstream of the inlet tip. However, the shroud does not incorporate sufficient leading edge bluntness to accommodate large incidence angles. Observations on a flight when tufts of yarn were attached to the shroud suggest that the sideslip angle may have been worse than expected at the shroud location (D. Friesen 1999, personal communication), and perhaps beyond the correction capability of the CAI's shroud. Using mean flow speeds in the various CAI sections, the estimated particle residence time in-

TABLE 1. Calculated CAI transmission efficiencies for supermicron particles.

Particle diameter (μm)	Transmission efficiency	
	Density = 1.0	Density = 2.0
2.0	N/A	56%
3.0	55%	40%
4.0	43%	28%
5.0	33%	21%
6.0	26%	18%

TABLE 2. Calculated transmission efficiencies for sample pickoff tubes.

Tube ID (cm)	Particle density g cm^{-1}	Particle diameter (μm) for transmission efficiency of		
		90%	50%	10%
0.46	1.0	2.7	6.1	9.1
	2.0	1.9	4.3	6.4
1.80	1.0	3.7	9.6	17.5
	2.0	2.6	6.8	12.4
2.92	1.0	4.8	12.2	22.3
	2.0	3.4	8.6	15.7

side the CAI (upstream of the sampling plane) is approximately 0.4 s. Therefore, sedimentation along the length of the CAI should be on the order of 0.001 m for a 10-μm, unit-density particle with a sedimentation velocity of 0.003 m s^{-1}. For these reasons, this work focuses on deposition at high Re and in bends as the most probable loss mechanisms for large particles within the CAI.

Many of the empirical studies of particle deposition due to turbulence are based on smaller tubes and substantially lower Reynolds numbers than occur within the CAI. However, one recent study that focuses on turbulent deposition in large transport tubes at moderately high Reynolds numbers (Muyshondt et al. 1996) can be used to estimate turbulent losses in the CAI. Turbulence intensity measurements described above show that flow characteristics at the sampling plane (Re = 77 000) are those of fully developed turbulent pipe flow. It is assumed here that the higher speed upstream sections, with Reynolds numbers over 100 000, can be treated in a similar manner. Using Eqs. (1)–(6) and (10) of Muyshondt et al. (1996), the transmission efficiency for the CAI was calculated as a function of particle size. Each section of the CAI was considered separately (and assumed to be cylindrical for the purpose of this computation), with the arithmetic mean of the inlet and exit diameter being used in the calculations for the short diffusing sections. Transmission efficiencies for each section were then multiplied to produce an overall transmission efficiency for the entire inlet length.

The experimental data and curve fit from the Muyshondt et al. study apply up to a Reynolds number of 5×10^4 and up to nondimensionalized particle relaxation times (τ^+) of 100. The curve fit produces unrealistic results for larger Re and τ^+. However, the experiments indicate that transmission efficiency is relatively constant for high Re and τ^+. Therefore, we set Re to 5×10^4 in the calculations, even though actual values in the CAI are somewhat higher (7.7 to 20 $\times$ 10^4). For the same reason, τ^+ was set equal to 100 for the first two sections of the CAI and for some of the larger particle sizes. Extrapolation of results to low τ^+ is much more uncertain than for high τ^+ (A. Muyshondt, 1999, personal communication), so we did not attempt to calculate efficiencies at τ^+ less than 1.0. This corresponds to unit-density particles 2.0 μm and smaller.

The results of these calculations are shown in Table 1 for atmospheric boundary layer values of 1000 mb and 293 K. Transmission efficiencies were calculated for particles with densities of 1.0 and 2.0 g cm^{-3}. Pure $(NH_4)_2SO_4$ has a dry particle density of 1.77 g cm^{-3}, while pure NaCl has a dry density of 2.16 g cm^{-3}. Hydrated aerosol particles will have densities between 1.0 and these values, depending on ambient conditions. A smooth curve fit through these points indicates a particle diameter transmitted with 50% efficiency, or ''cut-size,'' of 2.4–3.4 μm, depending on particle density. The greatest losses are in the long tubular section following the first diffuser, where the Reynolds number is still quite large. For 3 μm particles penetration is only 47% in this section, whereas it is >80% in all other sections. In retrospect, it may have been more effective to use one diffusing section rather than three separate sections. Downstream of the CAI sampling plane, particles are brought into the cabin through 90° bent tubes of various sizes. Since large particles can be deposited in bends even at relatively low airflow, transmission characteristics of various tubes used with the CAI were modeled. Calculations are from Cheng and Wang (1977) for the smallest tube (laminar tube flow) and from Pui et al. (1987) for the larger tubes (turbulent tube flow). The ratio of bend radius to cross-sectional radius for all tubes is within the range of these studies ($5 \leq R_{curve}/R_{tube} \leq 30$). A sampling plane velocity of 10 m s^{-1} and particle densities of 1.0 and 2.0 g cm^{-3} are assumed. Table 2 gives the diameter of particles that are transmitted with 90%, 50%, and 10% efficiency for the smallest, largest, and intermediate tube sizes. Inspection of Tables 1 and 2 shows that bend deposition is less a problem than turbulent deposition in the upstream horizontal sections of the CAI, but is still important, especially for the smallest tube size.

Laboratory tests with aerosols (uranine in dioctyl phthalate, ρ = 0.98 g cm^{-3}) produced by a Vibrating Orifice Aerosol Generator (VOAG) (model 3450, TSI Inc.) showed that the large pickoff tube (2.92 cm) and associated plumbing (used by UH for filter and impactor measurements) pass more than 90% of particles below 4 μm, with a 50% cut at $\approx$7 μm (Fig. 6). This indicates a sharper cutoff than predicted on Table 2, but is still greater than the predicted CAI transmission efficiency. Therefore, differences between measurements taken

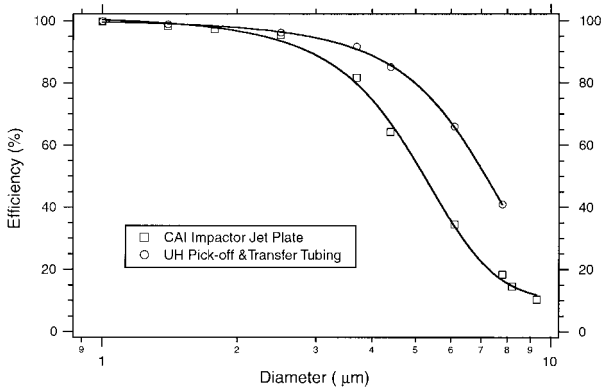

FIG. 6. Passing efficiency calibration data for the large (2.92 cm) pickoff tube and inlet system and for the CAI impactor assembly at design flowrates. Uranine/dioctyl phthalate aerosols of known size were produced in a vibrating orifice aerosol generator. Results show a cut-size diameter (50% efficiency) of 7 μm for the pickoff/transfer tubing and 5 μm for the impactor jet plate.

from samplers behind the CAI and those taken external to the aircraft can be attributed mostly to losses in the CAI and less to losses in plumbing downstream.

4. Transmission of submicron aerosol particles

a. Optical particle, counter measurements

During CAINE (Flight 12), measurements made with a PMS LAS-X Optical Particle Counter (OPC) on a 295-m tower, using no additional inlet, were compared with coincident measurements made with a similar counter behind the CAI as the C-130 flew by the tower. No significant difference was observed between the number concentration of particles larger than 0.32 μm measured behind the CAI and the number measured on the tower by the OPC. Since the number concentration was dominated by particles in the 0.32–0.48-μm size range, this indicates the CAI transmits these particles with high efficiency. Particle counts in the larger bins were too few to assess differences with statistical confidence.

b. Chemical measurements

To directly measure the passing efficiency of the CAI for various classes of particles, one must compare ambient aerosol concentrations with those measured behind the CAI. The difficulty, of course, is to measure the ambient concentration without inlet losses, thus providing the ambient reference value.

The University of Hawaii's external filter sampler (EXT) was used for this purpose. All particles lost from the airstream to the diffuser walls in this sampler are extracted and analyzed when the cone is removed from the aircraft following each flight. Operated isokinetically, the EXT sampler should have aspiration efficiency near unity. Since 1) the inlet tip is sealed except during sampling and 2) everything that enters the tip must be either on the cone or the filter immediately behind the cone, the external sampler provides a defendable reference bulk concentration of aerosols for comparison with samplers behind the CAI. The removable diffuser cone system is a modification of the inlet used in an earlier passing efficiency experiment (Huebert et al. 1990) and is similar to the aerosol filter inlet described by Sheridan and Norton (1998), which uses a removable filter cone behind the inlet orifice. The EXT sampler has been successfully deployed on the NCAR Electra during the Atlantic Stratocumulus Transition Experiment (ASTEX) (Huebert et al. 1996) and on the NCAR C-130 during ACE-1 (Huebert et al. 1998).

On Flight 13 of CAINE-II in the Gulf Mexico, windspeeds were low and sodium levels were barely above detection limit. APS particle size data behind the CAI confirmed the absence of larger particles. However, anthropogenic sulfate levels were very high. Since, in the absence of seasalt, sulfate is found primarily in the submicron aerosol, the sulfate data from this flight can be used to assess the transmission efficiency of the CAI for submicron aerosol. The external filter-plus-diffuser-cone measurement indicated that 9.2 ± 0.5 μg m^{-3} of sulfate was present in the ambient aerosol, while a filter behind the CAI measured 9.7 ± 0.5 μg m^{-3} (Table 3). Thus, within the uncertainty of the measurements, the CAI transmitted submicron sulfate particles with efficiencies near 100%.

5. Transmission of supermicron aerosol particles

a. C-130 Chemical measurements from CAINE-II and ACE-1

There is at least one way to measure a defendable bulk passing efficiency for the CAI: compare chemical concentrations collected downstream of the CAI with those measured by an external total aerosol sampler. During ACE-1 and the CAINE-II New Orleans flights, filter samples were collected from the UH external sampler and from both a filter and a single stage impactor (Tedlar substrate for particles >1 μm and Teflon backup filter) drawing air from the largest (2.92 cm) of the CAI pickoff tubes. In both CAINE-II and ACE-1 isokinetic flow was maintained in the external sampler and in all CAI pickoff tubes during sampling, except on Flight 16 of CAINE-II. During this flight the external sampler could not achieve isokinetic flow, apparently because the filter came from a batch with a higher than normal flow resistance.

The CAI impactor is designed to separate seasalt aerosol from submicron modes, increasing the measurement sensitivity for nonseasalt sulfate (NSS) in the submicron fraction. Since the 50% cut size for the jet plate is about 5 μm (Fig. 6), the impactor substrate represents particle mass in the 1–5-μm range and the backup filter collects the submicron modes. For CAINE-II and ACE-1 the impactor substrate and backup filter values have been

TABLE 3. C-130 chemical data from external and CAI samplers during CAINE-II.

	Na (μg m^{-3})			NSS (μg m^{-3})		
Flight	EXT	FIL	IMP	EXT	FIL	IMP
12	0.44 ± 0.03	0.07 ± 0.02	0.06 ± 0.02	4.37 ± 0.21	2.68 ± 0.14	1.84 ± 0.08
13	0.10 ± 0.02	0.02 ± 0.02	0.05 ± 0.02	9.18 ± 0.45	9.74 ± 0.49	9.68 ± 0.47
14C	—	0.17 ± 0.07	0.11 ± 0.07	—	9.20 ± 0.46	9.01 ± 0.44
14D	—	0.32 ± 0.06	0.27 ± 0.06	—	9.39 ± 0.48	9.13 ± 0.44
15	—	0.48 ± 0.03	0.28 ± 0.02	—	5.03 ± 0.26	5.02 ± 0.24
16	<7.9*	1.11 ± 0.06	0.98 ± 0.04	<9.1*	6.04 ± 0.32	6.03 ± 0.29

* Upper limit. Sampler flow was sub-isokinetic, so large particles may have been oversampled.
EXT = UH external total sampler.
FIL = Filter sample from the large (2.92 cm) pickoff tube on the CAI.
IMP = Impactor sample (substrate + backup filter) from the large (2.92 cm) pickoff tube on the CAI.

summed, representing the total aerosol mass less than 5 μm passing the CAI. Comparisons between the impactor and CAI filter therefore provide an estimate for the amount of aerosol greater than 5 μm that passed through the CAI inlet system and delivery tubes.

Chemical comparisons between the external sampler, the CAI filter (FIL), and the CAI impactor (IMP) during CAINE-II are shown in Table 3. Sodium is used as a surrogate for supermicron particles because most of the seasalt mass is larger than one micron (Huebert et al. 1998). In the marine boundary layer, Na_{FIL}/Na_{EXT} ratios less than one indicate the removal of seasalt, mostly by the CAI. As mentioned above, the impactor system has additional losses in the jet plate, removing some particles larger than about 5 μm (Fig. 6). Thus, the impactor and filter should be comparable in the absence of particles larger than 5 μm. When large particles are present we should find $Na_{EXT} > Na_{FIL} > Na_{IMP}$.

While CAINE-II was conducted in a marine region (the Gulf of Mexico), specifically to provide a seasalt aerosol for this test, unusually low wind speeds resulted in low concentrations of Na^+ on all but Flight 16. However, data from Flights 12 and 16 convincingly show that most of the sodium mass does not pass the CAI. FIL and IMP samples account for only 10%–20% of the sodium mass observed in the reference EXT sampler. Close agreement between FIL and IMP samples implies that few particles passing the CAI are larger than 5 μm (the impactor jet plate cutoff diameter).

This same result was found for a much larger number of samples in ACE-1, under clean background conditions with high wind speeds. These results (Fig. 7) also show that the vast majority of the sodium mass is lost in the CAI and never reaches the impactor. The IMP to EXT concentration ratios of Na^+, Cl^-, SO_4^{2-}, and NSS during clean baseline conditions were 0.2 ± 0.1, 0.2 ± 0.1, 0.4 ± 0.2, and 0.8 ± 0.3, respectively. The evidence from both flight programs points to losses of 70%–90% for bulk sea salt mass in the CAI.

b. Comparisons with ambient size distributions from ACE-1

It is necessary to know the size dependence of the inlet efficiency to know what size classes of data from the CAI are defendable. One approach is to determine the diameter below which 10%–20% of the sea salt mass resides, since this is the fraction seen to pass the CAI-based on EXT and IMP filter data. The IMP to EXT ratio, applied to independently measured or calculated sea salt distributions (e.g., during ACE-1) can provide an estimate of the CAI cutoff size. Even if the actual cutoff is not sharp, this derived size should be near the 50% cut size (the diameter at which 50% of particle mass penetrates the inlet).

The ACE-1 field program was conducted in the Southern Hemisphere near Tasmania. In the marine boundary layer the airborne samplers often encountered very clean air with a supermicron mode dominated by sea salt particles (baseline conditions). At the same time, size resolved chemical data was collected at Cape Grim, Tasmania using a Multiple Orifice Uniform Deposit Impactor (MOUDI). Average baseline distributions for Na^+, Cl^-, and SO_4^{2-} during ACE-1 are shown in Fig. 8. If we assume that MOUDI data accurately represent the average ambient size distributions for these species and that the C-130 external filter sampled the same distribution, an estimate for the CAI cut size can be derived from a consideration of the IMP to EXT concentration ratios from ACE-1. The shaded portion of each distribution in Fig. 8 shows the fraction corresponding to the CAI impactor concentration. The upper limit of this area is an estimate for the CAI cut size. This analysis again points to a limit of about 2–4 μm for the CAI cut size.

Since the MOUDI itself has inlet losses, however, it is possible the distributions shown in Fig. 8 have also undersampled some of the largest particles. Also, some portion of the observed inlet loss occurs in the pickoff and transfer tubing (7 μm cut size for $\rho \approx 1.0$ g cm^{-3} particles). Nevertheless, the conclusion that few particles larger than 2–4 μm are able to pass the CAI is consistent with other filter data and modeling estimates presented above.

c. Particle size distribution measurements

During CAINE-II an aerodynamic particle sizer (APS) measured the supermicron aerodynamic particle

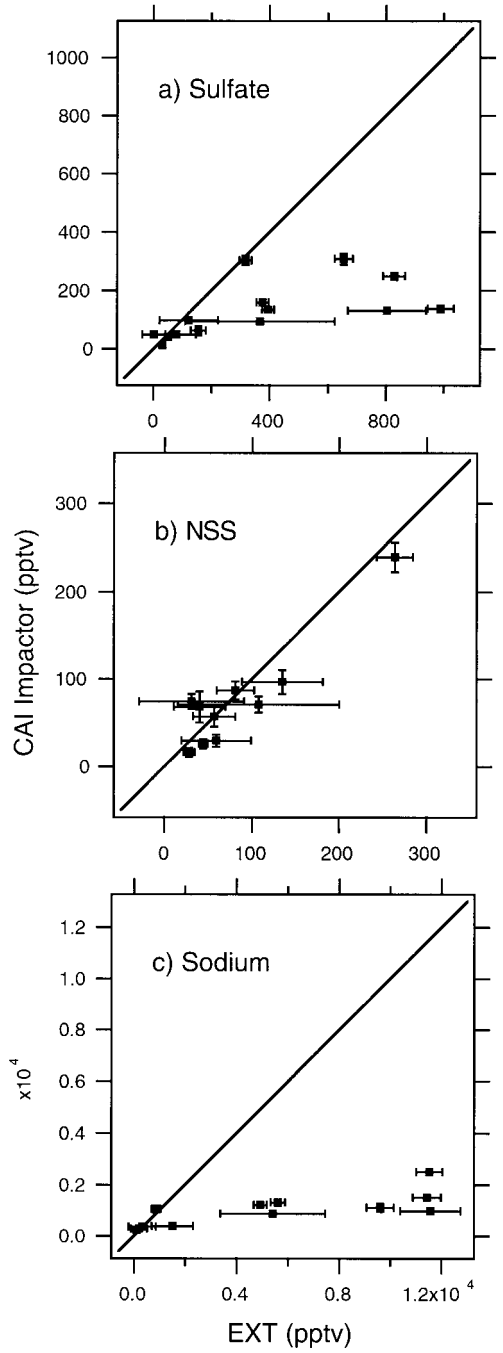

FIG. 7. Comparisons of simultaneous samples of (a) total sulfate, (b) nonseasalt sulfate (NSS), and (c) sodium measured on the external aerosol sampler and an impactor installed behind the CAI during ACE-1. Impactor data represent the sum of the substrate and backup filter values (all particles <5 μm). Measurements of NSS, which is typically found on submicron particles, agree well. Total sulfate and sodium, more abundant in the supermicron mode, are undersampled by the CAI impactor, implying significant losses of up to 90%.

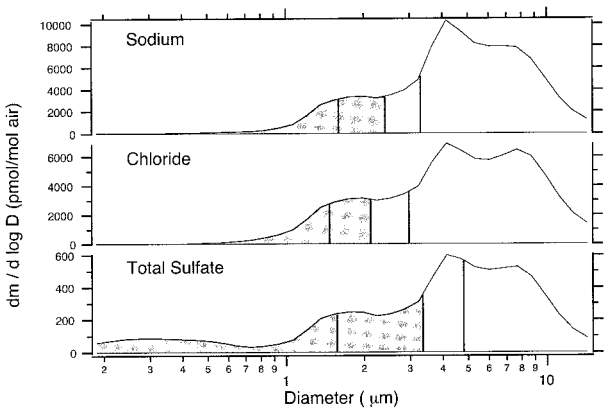

FIG. 8. ACE-1 MOUDI data for Na^+, Cl^-, and SO_4^{2-} from Cape Grim, Tasmania under clean baseline conditions. The mass distributions are Twomey inversions (Winklmayr et al. 1990) of averages from 5 sequential samples over 5 days. Shaded areas compare the mean amount (± 1 σ) measured by the CAI impactor (IMP) as calculated from the IMP/EXT ratios for C-130 samples obtained under similar clean baseline conditions. The upper limit for the shaded area is an estimate for the ''cut size'' of the CAI.

size distribution passing through the CAI and associated plumbing, just upstream of impactor and filter samplers. Because of the low flight altitude (100 ft), cabin and external temperatures were identical. Therefore, relative humidity was constant and RH corrections to the APS size distributions were not necessary. APS data in Fig. 9 show that a few particles of diameter >4 μm do indeed pass the CAI. On Flight 16 the average APS volume integral was 9.58 μm^3 cm^{-3} air. Assuming this is purely sea salt aerosol, using a wet particle to dry particle mass ratio of 4.27 at 80% RH (Tang et al. 1997), and assuming a typical wet particle density of 1.2 g cm^{-3} for supermicron sea salt (Howell 1996; Howell and Huebert 1998), the measured APS volume is equivalent to a sodium concentration of 0.93 μg m^{-3} of air. Thus the APS data predicts virtually the same sodium concentration that the CAI filter and impactor samplers measured on Flight 16 (Table 3: 1.11 $\pm$ 0.06 and 0.98 $\pm$ 0.04 μg m^{-3}, respectively). We therefore assume that the APS data accurately represent the particle size distribution passing the CAI. To compute efficiency versus size, we now consider approaches to determining the ambient size distribution for comparison with the CAI distribution measured by the APS.

Because it does not require an inlet, the FSSP-300 was used to measure the reference ambient particle size distribution. However, the FSSP measurement relies on Mie scattering intensity, which does not have a single-valued relationship to particle size and varies significantly as a function of refractive index. Assuming a value for the refractive index of the particles appropriate for sea salt (Howell and Huebert 1998), a size distribution was calculated from the FSSP output (Fig. 9). Aerosol density representative of sea salt particles (Howell 1996; Howell and Huebert 1998) was used to

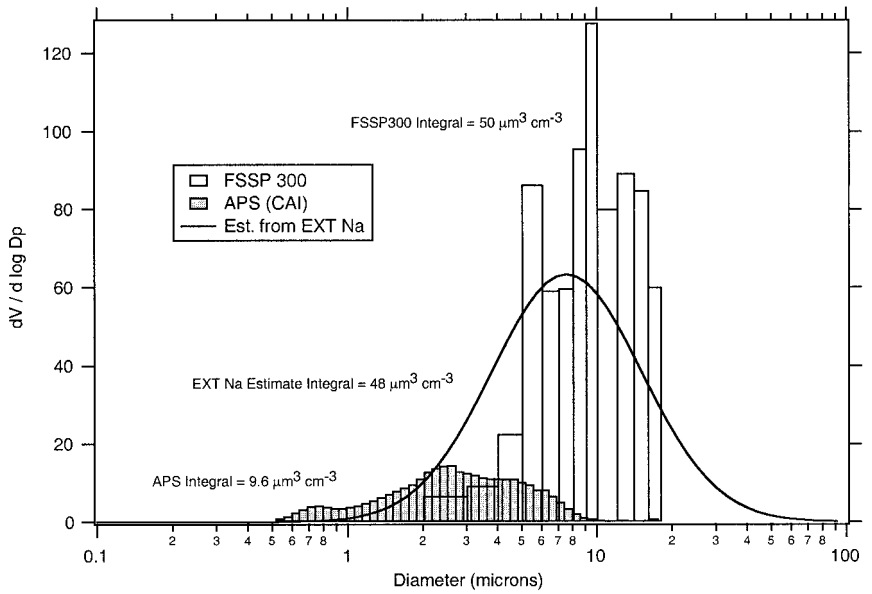

FIG. 9. CAINE-II (Flight 16) aerosol volume distributions measured behind the CAI by an Aerodynamic Particle Sizer (APS), measured externally by a forward scattering spectrometer probe (FSSP-300), and a lognormal estimate for ambient supermicron sea salt volume distribution derived from EXT sodium (mean $\approx$ 7 μm, σ = 2, area = 48 μm^3 cm^{-3}).

convert the aerodynamic sizes measured by the APS into geometric sizes comparable to those derived from the FSSP.

FSSP measurement uncertainties are discussed in detail by Baumgardner et al. (1992). Imprecision in measuring the concentration of particles can arise from uncertainties in the optical sample volume, detection errors caused by coincidence, deadtime losses, and poor sampling statistics. The size of a detected particle deviates from ideal because of variations in the intensity of the laser beam; electronic time response of the probe; particle asphericity; temperature sensitivity of the photodetectors; and calibration uncertainties arising from the complicated relationship between scattering intensity, particle size, and refractive index. In addition to the uncertainties in FSSP-300 measurements discussed by Baumgardner et al. (1992), another source of sizing error may arise from particle coincidence. When aerosol concentrations are relatively high ($>$500 cm^{-3}) the probability of particles coincident in the probe's sample volume becomes significant. The effect will be to underestimate the number concentration but oversize some fraction of the particles. This may be responsible for some of the apparent mass above 10 μm in the FSSP trace in Fig. 9. If real, this effect could at least lead to broadening of the distribution around this peak.

FSSP and APS data shown in Fig. 9 illustrate the differences between the ambient size distribution and the distribution passing the CAI. While the shape of the FSSP distribution is a bit rough, the ratio of APS to FSSP volume is about 0.2, supporting the observation from chemical data that less than 20% of the supermicron sea salt mass passes the inlet system. Also, the FSSP volume integral is very close to the estimated supermicron particle volume estimated in the next section from the measured external Na concentration.

d. Size-dependent efficiency from CAINE-II sodium and APS data

The external Na concentration allows us to calculate a volume for the ambient sea salt distribution. Continuing with the assumption that the supermicron aerosol is seasalt, the difference in sodium concentration between the external sampler and the impactor backup filter (representing only submicron particles) on Flight 16 can be used to estimate an integrated volume for the ambient supermicron aerosol. Using the same set of assumptions as above, the estimated sea salt particle volume obtained from EXT sodium is $\approx$77 μm^3 cm^{-3}.

Reasonable assumptions for the geometric mean and standard deviation are required to calculate a lognormal distribution for the ambient supermicron mode. In Figs. 9 and 10 a geometric mean ($\approx$7 μm) and standard deviation (σ = 2) were chosen such that the calculated lognormal distribution more or less coincides with the APS-measured distribution in the 1–2-μm region. These statistics are representative of typical values for the supermicron seasalt mode (O'Dowd et al. 1997; Seinfeld and Pandis 1998, chapter 7). However, since the EXT sampler was sub-isokinetic for Flight 16 (62 m s^{-1} inlet flow vs 108 m s^{-1} airspeed) an additional correction is necessary. Stokes numbers were calculated (Huebert et al. 1990) for the entire particle size range using the

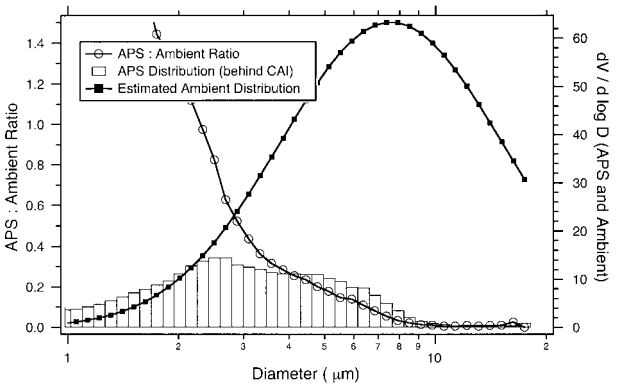

FIG. 10. Ratio plot of APS dV/d log D to the estimated ambient dV/d log D obtained from EXT sodium. Assuming the shape of the estimated ambient distribution is reasonable, the cut size (50% efficiency) is 2–3 μm; however, transmission is still about 10% efficient out to 6–7 μm. Efficiencies greater than 1 at smaller diameters is an artifact resulting from the tail of a large submicron mode sensed by the APS but not included in the modeled distribution.

corrected airspeed (108 m s^{-1}) and a sea salt density of 1.2 g cm^{-3}. The empirical relationship determined by Zenker (Fuchs 1975) was used to correct for sub-isokinetic sampling conditions across the particle size range. The resulting corrected estimate for the ambient supermicron seasalt mode volume is 48 μm^3 cm^{-3}. The lognormal distribution plotted in Figs. 9 and 10 was fit to this estimated volume integral. The APS-measured volume (9.58 μm^3 cm^{-3}) amounts to only about 20% of this value, which is consistent with the bulk chemical data.

If we divide the volume in each APS size interval by the corresponding volume from the lognormal ambient estimate, the resulting ratio is an estimate of the overall passing efficiency versus size (Fig. 10). The calculated efficiency is greater than 1 at the smaller sizes. This is an artifact arising because the sea salt mode is not the only contributor to the APS volume at those sizes. There was a very large sulfate-rich accumulation mode near New Orleans that the APS sensed below 1 μm. The modeled volume distribution based on Na chemistry considers only sea salt and does not include estimated contributions from the tail of a submicron mode and will thus underestimate the volume at smaller sizes.

The details of this estimated passing efficiency curve obviously depend on the geometric mean and sigma selected for the lognormal distribution, which in this case are chosen somewhat arbitrarily. But its form should be robust: high transmission efficiency prevails up to a diameter of about 2 μm, above which passing efficiency drops significantly. However, the cutoff is not sharp. A few 10-μm particles are able to penetrate the CAI, but with an efficiency of at most a few percent. Below about 7 μm, we attribute most of this loss to the CAI itself. Above that size, however, the delivery tubing would also tend to remove large particles that had survived the CAI. The 50% cut size of about 3 μm based on a comparison to the APS data is consistent with both the calculations (section 3) and the simple chemical data (Fig. 8).

6. Conclusions

Based on both in-flight measurements and a fluid dynamics model, airflow in the CAI is similar to fully developed pipe flow. Turbulence intensities near the sampling plane are in the range of 7%–9%. The nature of the flow was insensitive to aircraft attitude, but reflected changes in airspeed. A small boundary layer suctions scheme does not measurably affect the flow or decrease turbulence.

The uniformity of the flow and thus the ability of users to isokinetically sample air from the CAI depends on maintaining the design flow through every pickoff tube. Distortions of the velocity field are pronounced when suction to one tube is shut off. Each user must therefore plan for a bypass flow when his or her instrument's flow is shut off.

Data from CAINE and CAINE-II showed that the CAI samples submicron aerosol with near-unit efficiency. However, chemical data from both ACE-I and CAINE-II clearly indicate that very little of the sea salt (coarse mode) mass is transmitted by the CAI to instruments inside the aircraft. From the ACE-I EXT and CAI filter chemistry, it appears that 70%–90% of the seasalt mass is unable to pass the CAI and reach samplers inside the fuselage. The ''50% cut size'' for the CAI is about 3 μm for humid sea salt particles with density of 1.2 g cm^{-3}. Cut size conclusions are supported by modeled particle transmission efficiencies for the CAI and are consistent with two evaluations of other inlets (Huebert et al. 1990; Sheridan and Norton 1998).

The loss of particle mass becomes very significant above 3 μm, but the cut size is not sharp. A small amount of material at sizes considerably larger than 3 μm is clearly seen in the APS data. The uncertainty in the derived efficiency versus size is largely due to the difficulty of measuring an unbiased ambient particle spectrum. Clearly, another approach to analyzing optical particle counter data in the supermicron size range is needed to facilitate analyses of this type. Algorithms for extracting accurate size distributions by inverting all the information contained in the FSSP scattering intensity measurements could possibly achieve the needed precision but have yet to be developed.

The principal value of the multiuser Community Aerosol Intel system for NCAR's C-130 is that it decelerates air with no curves until the velocity has been reduced to 10 m s^{-1}. It then supplies a large quantity of uniformly modified air (after turbulent losses) to all users, enabling valid closure experiments. For submicron particles its efficiency is near unity. Unfortunately, this large inlet suffers from large particle losses, as do all turbulent decelerating inlets.

Acknowledgments. This work was supported by National Science Foundation Grant #ATM-9813515 and NCAR's Research Aviation Facility. Particular thanks are due to Dave Carlson, Dick Taylor, and the entire staff at NCAR's Research Aviation Facility, whose flexibility, dedication, and good humor make this kind of work productive and enjoyable. We especially acknowledge the work of Diane Rogers in designing the CAI.

REFERENCES

Baumgardner, D., and B. Huebert, 1993: The airborne aerosol inlet workshop: Meeting report. *J. Aerosol Sci.*, **24,** 835–846.

——, J. E. Dye, B. W. Gandrud, and R. G. Kollenberg, 1992: Interpretation of measurements made by the Forward Scattering Spectrometer Probe (FSSP-300) during the Airborne Arctic Stratosphere Expedition. *J. Geophys. Res.,* **97,** (D8), 8035–8046.

Cheng, Y.-S., and C.-S. Wang, 1977: Inertial deposition of particles in a bend. *Aerosol Sci. Technol.,* **6,** 129–145.

Fuchs, N. A., 1975: Sampling of aerosols. *Atmos. Environ.,* **9,** 697–707.

Howell, S. G., 1996: Determination of marine aerosol composition, mass distribution, and optical properties. Ph.D. dissertation, University of Rhode Island, 282 pp.

——, and B. J. Huebert, 1998: Determining marine aerosol scattering characteristics at ambient humidity from size-resolved chemical composition. *J. Geophys. Res.,* **103,** 1391–1404.

Huebert, B. J., G. Lee, and W. L. Warren, 1990: Airborne aerosol inlet passing efficiency measurement. *J. Geophys. Res.,* **95,** 16 369–16 381.

——, L. Zhuang, S. Howell, K. Noone, and B. Noone, 1996: Sulfate, nitrate, methanesulfonate, chloride, ammonium, and sodium measurements from ship, island, and aircraft during the Atlantic Stratocumulus Transition Experiment/Marine Aerosol Gas Exchange. *J. Geophys. Res.,* **101,** 4413–4423.

——, and Coauthors, 1998: Filter and impactor measurements of anions and cations during the First Aerosol Characterization Experiment (ACE-1). *J. Geophys. Res.,* **103,** 16 493–16 509.

Houghton, J. T., L. G. Meira Filho, J. Bruce, H. Lee, B. A. Callander, E. Haites, N. Harris, and K. Maskell, Eds., 1995: *Climate Change 1994: Radiative Forcing of Climate Change and An Evaluation of the IPCC IS92 Emission Scenarios.* Cambridge University Press, 339 pp.

Muyshondt, A., N. K. Anand, and A. R. McFarland, 1996: Turbulent deposition of aerosol particles in large transport tubes. *Aerosol Sci. Technol.,* **24,** 107–116.

O'Dowd, C. D., M. H. Smith, I. E. Consterdine, and J. A. Lowe, 1997: Marine aerosol, sea-salt, and the marine sulphur cycle: A short review. *Atmos. Environ.,* **31,** 73–80.

Okazaki, K., R. W. Weiner, and K. Willeki, 1987: Non-isoaxial aerosol sampling: Mechanisms controlling the overall sampling efficiency. *Environ. Sci. Technol.,* **21,** 183–187.

Pui, D. Y. H., F. Romay-Novas, and B. Y. H. Liu, 1987: Experimental study of particle deposition in bends of circular cross section. *Aerosol Sci. Technol.,* **7,** 301–315.

Seinfeld, J. H., and S. N. Pandis, 1998: *Atmospheric Chemistry and Physics.* John Wiley & Sons, Inc., 1326 pp.

Sheridan, P. J., and R. B. Norton, 1998: Determination of the passing efficiency for aerosol chemical species through a typical aircraft-mounted, diffuser-type aerosol inlet system. *J. Geophys. Res.,* **103,** 8215–8255.

Tang, I. N., A. C. Tridico, and K. H. Fung, 1997: Thermodynamic and optical properties of sea slat aerosols. *J. Geophys. Res.,* **102,** 23 269–23 275.

Torgeson, W. L., and S. C. Stern, 1966: An aircraft impactor for determining the size distributions of tropospheric aerosols. *J. Appl. Meteor.,* **5,** 205–210.

Twohy, C. H., 1998: Model calculations and wind tunnel testing of an isokinetic shroud for high-speed sampling. *Aerosol Sci. Technol.,* **29,** 261–280.

Winklmayr, W., H.-C. Wang, and W. John, 1990: Adaptation of the Twomey algorithm to the inversion of cascade impactor data. *Aerosol Sci. Technol.,* **13,** 322–331.